Nuclear Instruments and Methods in Physics Research A323 (1992) 229–235
North-Holland

NUCLEAR
INSTRUMENTS
& METHODS
IN PHYSICS
RESEARCH
Section A

A microstrip gas chamber with true two-dimensional and pixel readout

F. Angelini, R. Bellazzini, L. Bosisio, A. Brez, M.M. Massai, A. Perret [1], G. Spandre and M.R. Torquati

INFN-Pisa and University of Pisa, Via Livornese 582-I-56010 S. Piero a Grado, Pisa, Italy

A true two-dimensional μstrip gas chamber has been constructed and successfully tested. This new detector has an effective substrate thickness of less than 2 μm. An ion implanted oxide layer of 1.8 μm thickness provides the necessary insulation between the front and back plane and permits collection on the back electrodes of a large fraction of the induced charge. The back electrode signal is used to measure the coordinate along the anode strips ($X-Y$ readout) or to provide true space points (pixel readout). Very good imaging capabilities have been obtained in both cases. A flux of 10^7 particles/mm^2 s has been measured without significant gain loss. No charging effect has been observed after three days continuously running at a flux of 10^4 particles/mm^2 s, while a 15% gain loss, probably due to ageing effects, has been measured after collection on the strips of a charge corresponding to the more than six years of running at the design luminosity of LHC, at 50 cm from the beam axis.

1. Introduction

Since its appearance [1–3] in the scenario of new detectors developed for high energy physics experiments at the future supercolliders (LHC, SSC) the μstrip gas chamber (MSGC) has been show to be a highly competitive device for its characteristics of high rate capability, very good spatial resolution, radiation resistance, simplicity and low cost.

Because of these features, it was quite soon used to track particles in a hadron spectroscopy experiment at the CERN-SPS [4] in the configuration of crossed pairs of detectors with orthogonal anode strips.

Although conceived as a one-dimensional detector, several authors [1,5] have considered the possibility of two-dimensional readout by suitably stripping the back plane, but practical detectors (i.e. with equal resolution for both the coordinates) could not be built, up to now, because of the very small signal available on the back electrodes. These electrodes are indeed quite far (typically 500 μm) from the anode strips and therefore electrically shielded by the much closer cathode strips. As shown in this paper, only a substantial development of the technology employed to build the detector allowed us to develop a device with a true two-dimensional readout. In this new type of detector the structure of the alternating cathode and anode μstrips is separated from the back plane by a thin (1.8 μm) insulating silicon oxide layer. The very small distance between anode and back plane results in inducing on it a large fraction of the charge delivered in the avalanche process. In the new electrode geometry it is the back plane that is now shielding the cathode strips which are much farther (typically 60 μm) from the amplifying electrode.

As already shown in a previous paper [6], the extremely small thickness of the oxide layer, which has a very high dielectric strength (around 1 kV/μm), causes the potential of the back electrode to affect strongly the operation of the chamber and allows to reach a gain of 10^4 at low working voltages easily.

2. The detector structure

Fig. 1 shows a cross section of the detector's internal structure. Moving from bottom to top we recognise:

i) the quartz substrate (500 μm thick), which acts only as mechanical support onto which a Ti film (metal 1, 0.2 μm thick) has been deposited. The Ti film was engraved using a UV lithographic technique to realise the readout structure of the back electrode;

ii) the 1.8 μm thick SiO_2 layer (Intermetal Oxide), obtained by chemical vapour deposition (CVD). It represents the effective substrate thickness and was implanted with a dose of 5×10^{16} boron ions/cm^2 to control charging effects;

iii) an Al film (metal 2, 2 μm thick) deposited onto the oxide layer below and onto which the anode-cathode microstrip structure was engraved;

iv) the gas gap (3 mm) which acts as active medium;

v) the drift electrode that defines the region of collection of the primary ionisation.

[1] CSEM – Neuchatel, Switzerland.

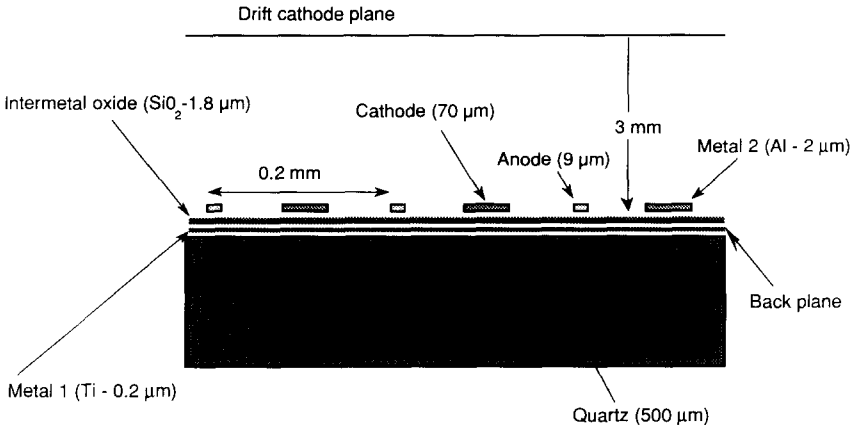

Fig. 1. Cross section of the detector internal structure.

The choice of the electrode structure for the back plane is almost free in shape (X, Y, ρ, ϕ, pad, pixel, small angle stereo, etc.) and sampling pitch (down to 50 μm). In the present work two different solutions are reported: pixels and strips.

a) The pixel structure is an 8×8 matrix of 1 mm^2 pads with a separation of 6 μm between them. In this electrode configuration the true two-dimensional read-out capability, accomplished through the collection of the signal from the pads (held at 0 V), is accompanied by the self-triggering capability due to the collection of the OR signal from the anode strips (held at positive potential).

b) The strip structure is a sequence of equipotential strips, 200 μm wide, 6 μm apart and orthogonal with respect to the anode strips. In this second configuration the anodes are at 0 V, while the back electrodes are connected to a negative potential through 1 MΩ polysilicon resistors. The small signal available on the side cathode strips can be used for triggering purposes only at high gain or when working with a large primary ionisation (for 8 keV X-ray detection, for example).

In both cases the separation of a few microns between pads or strips has produced no spatial modulation of the gain and a rather modest cross-talk level ($< 5\%$).

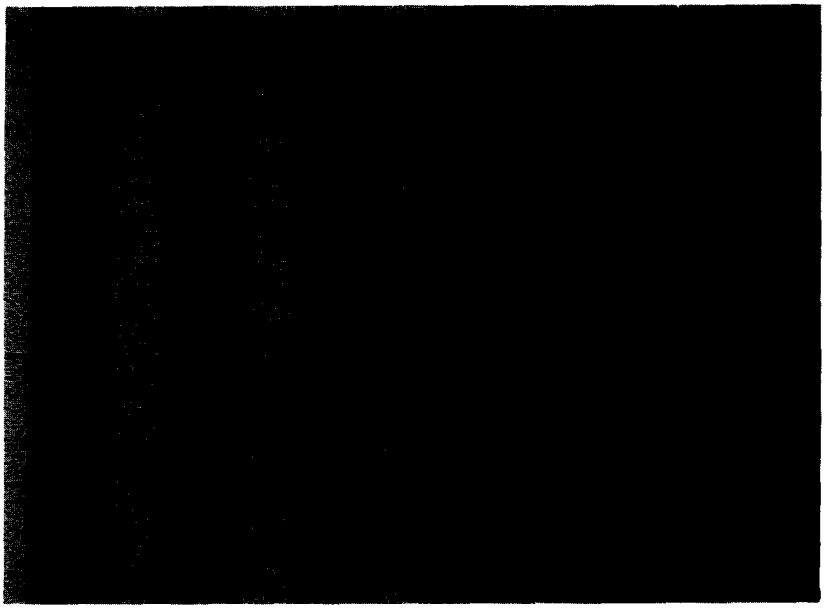

Fig. 2. Microphotograph of the detector with the strip structure for the back electrode.

A microphotograph of the X–Y structure is shown in fig. 2. This configuration is optimised to provide equal spatial resolution for both the coordinates.

3. The detector characteristics

Fig. 3a shows the signals obtained from the OR of the anode strips when the detector was illuminated with the Cu K_α line produced by an X-ray tube. The photopeak and the argon escape peak, at 8 and 5 keV respectively, are clearly distinguishable indicating the good energy resolution of this class of detectors. Because the range of the 8 keV photoelectron is rather large compared with the anode pitch, the good energy resolution is also a clear demonstration of the full electron collection efficiency. Fig. 3b shows the signal from the anode strips and from the corresponding pixel hit when the 8 keV X-ray beam was collimated to a 0.2

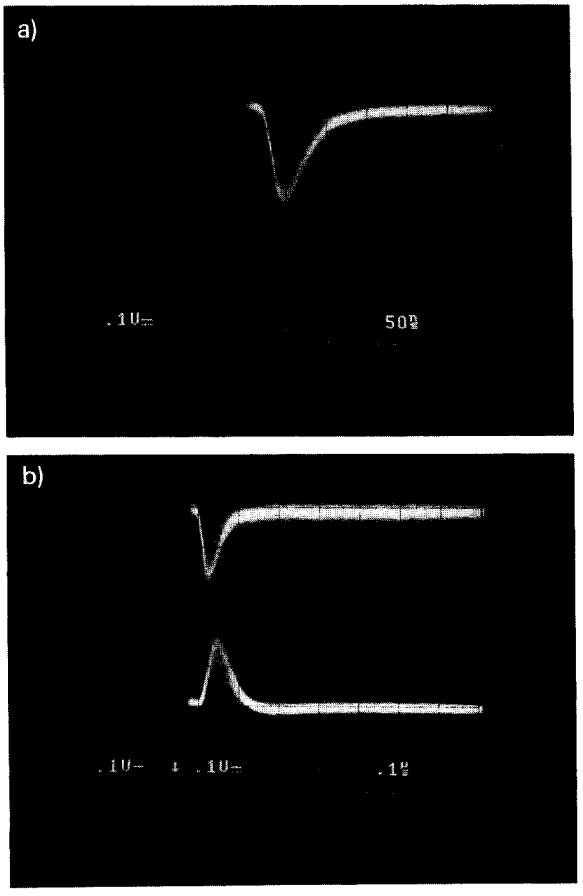

Fig. 3. (a) Signal obtained from the OR of the anode strips. (b) Signal obtained from the OR of the anode strips (upper trace) and from one pad (low trace). An 8 keV X-ray beam, collimated at 0.2 mm^2, illuminates the detector.

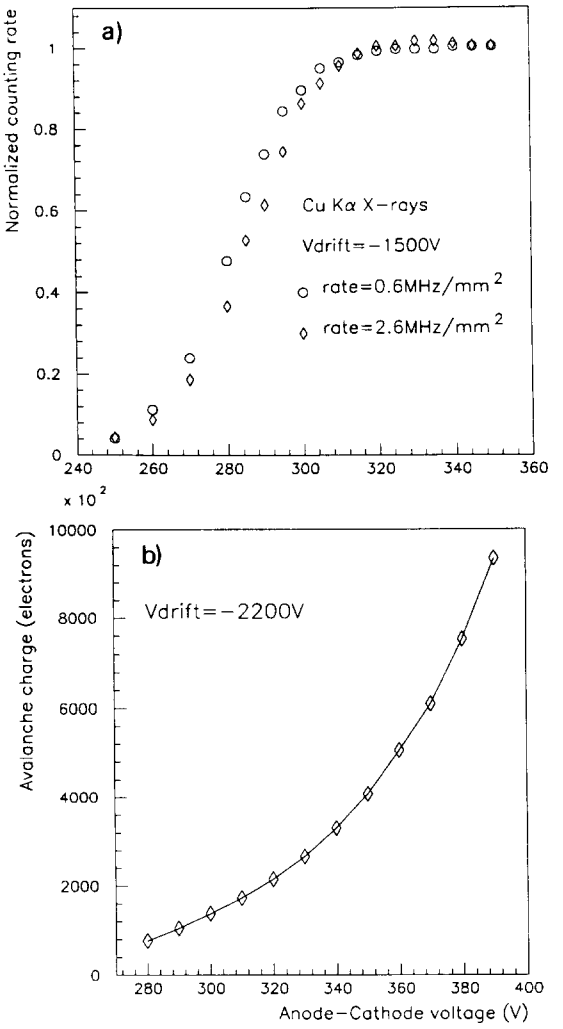

Fig. 4. (a) Plateau curve (singles) at two different values of the X-ray flux. (b) Total charge in the avalanche as a function of the anode voltage.

mm^2 spot. The shape and amplitude of both signals are almost equal. One should note the fast peaking time of the signals (20 ns). In all the measurements the gas mixture was Ar(90%)–DME (10%).

The dependence of the counting rate (singles) on the anode voltage has been studied, for the pixel structure, at two different values of the X-ray flux (0.6 and 2.6 MHz/mm^2). As is shown in fig. 4a the plateau is reached in both cases at a working voltage of about 310 V, the drift voltage being 1500 V negative and all the other electrodes grounded. This anode–cathode potential difference is much lower and therefore much safer than the one needed for thick detectors.

Fig. 4b shows the total charge delivered in the avalanche, as a function of the anode voltage.

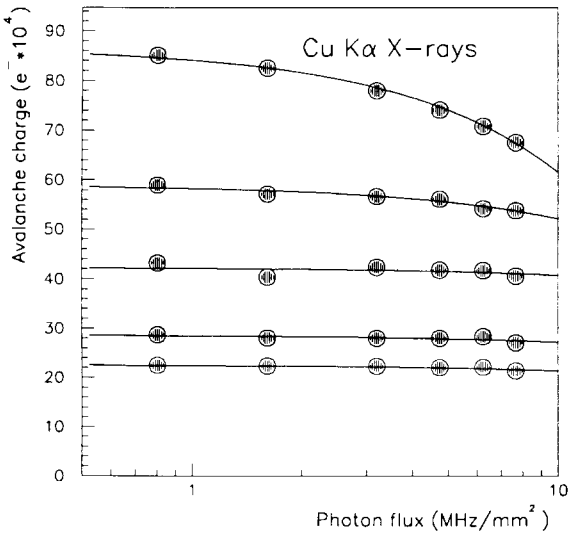

Fig. 5. Dependence of the total charge in the avalanche with the rate at several gas gains.

To study the rate capability of the detector we have measured the total charge in the avalanche as a function of the incoming flux at several gas gains (see fig. 5). With an avalanche charge of 6×10^5 electrons, no appreciable variation of the gas gain has been observed up to an extremely high value of the rate (> 7 MHz/mm^2). Some loss of gain can be observed at this rate only at an avalanche charge approaching 10^6 electrons.

A crucial point connected with the kind of substrate adopted, in our case represented by the SiO_2 layer, is determined by the so-called charging-up effect [9], namely a time-dependent modification of the gain due to the charging of substrate surface.

To study this problem, a long-term measurement of the average value of the anode pulse amplitude has been carried out. Fig. 6 shows the mean amplitude monitored over a period of more than three days of continuous running at an X-ray flux of 10^4 particles/mm^2 s. This flux is what is expected at LHC at 50 cm from the beam axis. No significant gain variation has been observed, confirming that ion implantation is a very effective technique to avoid surface charging [6]. Another important factor which has to be taken into account when considering a possible application of these detectors at high luminosity colliders is the ageing effect, i.e. the deterioration of the detector response when continuously exposed to a high flux of charge particles. A reduction of 15% of the average value of the pulse amplitude, together with some degradation of the energy resolution, has been observed (fig. 7) after the exposure to a flux of 10^6 particles/mm^2 s for a period corresponding to an integrated charge of 16×10^{-3} C/cm. This integrated flux is equivalent to more than six years of running at the design luminosity of LHC [10], at 50 cm from the beam axis. The gain reduction is a local effect. This is shown in fig. 7 by the recovery of the full gain when the beam

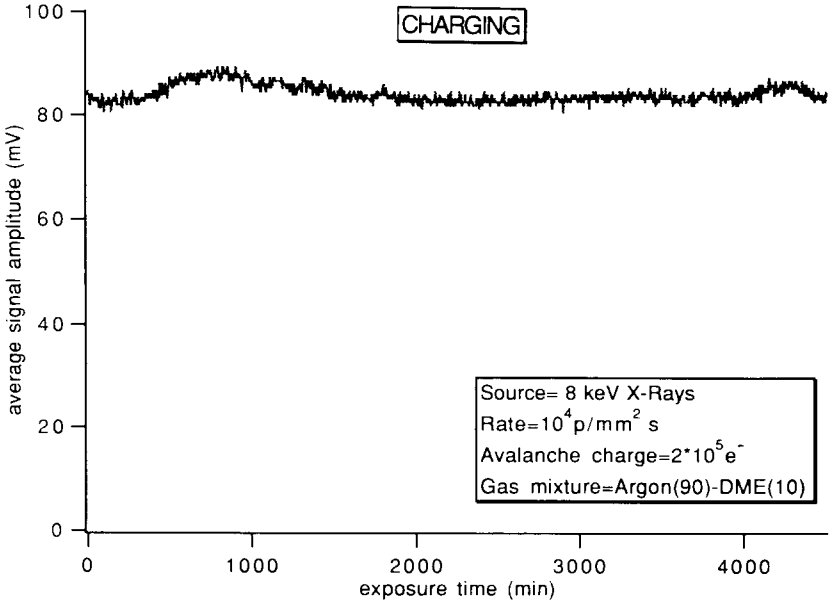

Fig. 6. Dependence of the average amplitude of the anode signal with time.

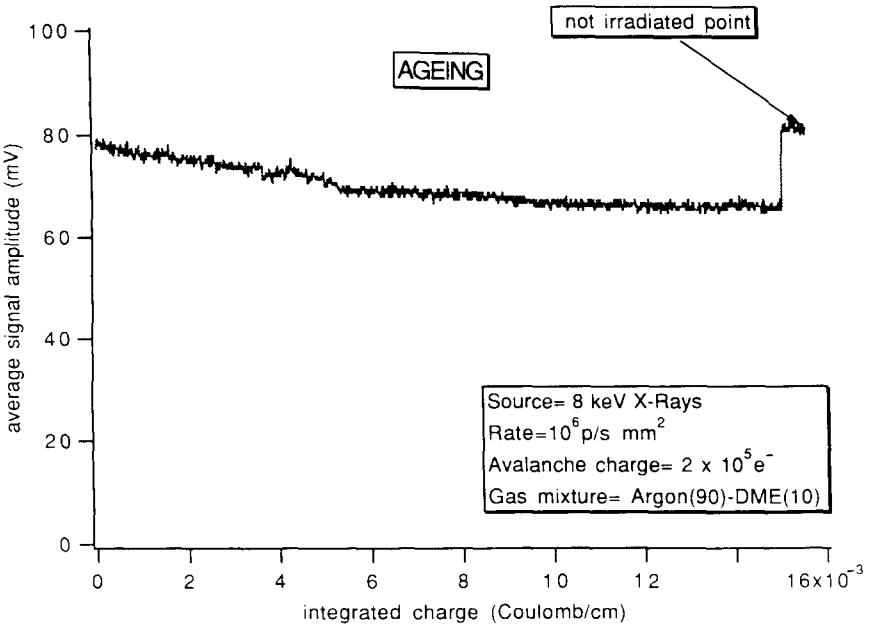

Fig. 7. Dependence of the average amplitude with integrated charge.

spot was moved a few mm along the same strips to a point not previously irradiated. At the irradiated point the recovery of the original gain was obtained with an increase of 10 V of the anode–cathode potential difference. This preliminary ageing test has been performed at low gas gain (around 10^3) and with an aluminum entrance window. Both conditions are known to favor ageing [7]. More detailed studies at different gains and with different materials are planned for the next future.

The detector imaging capabilities have been tested for both readout schemes.

Fig. 8 shows the position reconstruction capability of the pixel structure. The image has been obtained moving with 1 mm step the X-ray beam that was collimated at 1 mm^2 and plotting the isocount lines. The beam line was adjusted to center the pad.

To verify the imaging capability of the strip structure a mask, made of 39 holes of 0.5 mm diameter each with a minimum separation of 0.3 mm, and arranged to

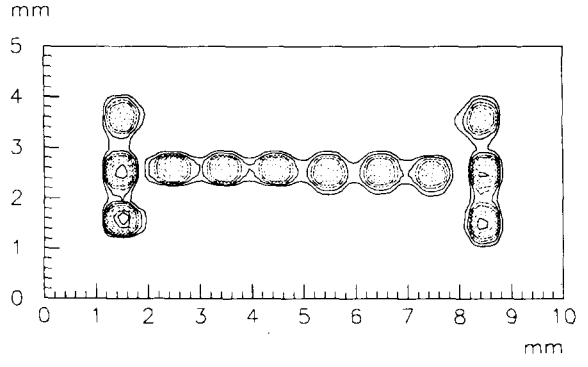

Fig. 8. $X-Y$ reconstruction capability in the case of the pixel structure.

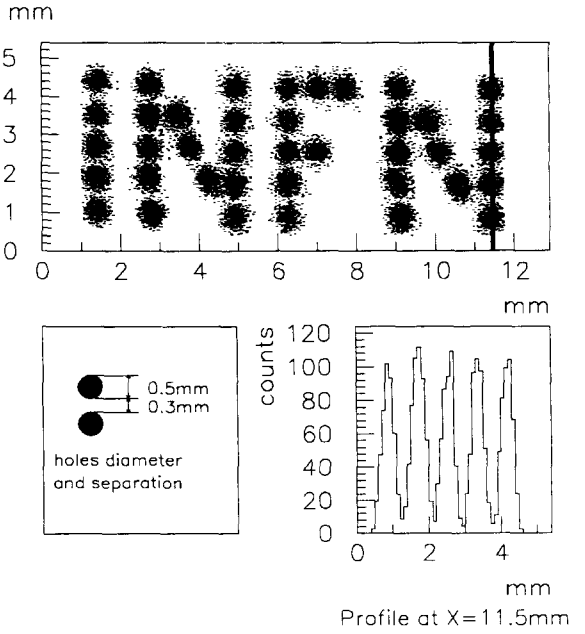

Fig. 9. Reconstructed image of a resolution mask obtained with the strip structure for the back electrode.

from the word INFN, was uniformly irradiated with the 8 keV X-ray tube. The X–Y coordinates were obtained by computing the center of gravity of the pulse height distribution. Fig. 9 shows the reconstructed image together with a profile across five holes. Each hole is perfectly resolved at the base. A spatial resolution of 160 μm, determined completely by the range of the 8 keV photoelectron has been evaluated for both the coordinates. With minimum ionising particles the spatial resolution is expected to be around 30 μm for both the coordinates as already measured in a test beam for the coordinate orthogonal to the anode strips [3,7].

The correlation function between the amplitude of the signal from anode strips and back strips is reported in the scatter plot of fig. 10a. Fig. 10b shows the distribution of the relative differences between back and anode strips pulse heights. The RMS of the distribution is only 6%. This strong correlation can be used to solve ambiguities when more than one particle crosses the detector at the same time.

A more complicated test of the imaging capability of the device is shown in fig. 11. It shows the X-ray image of a tiny golden earring having the shape of a swallow with 9 mm as maximum length.

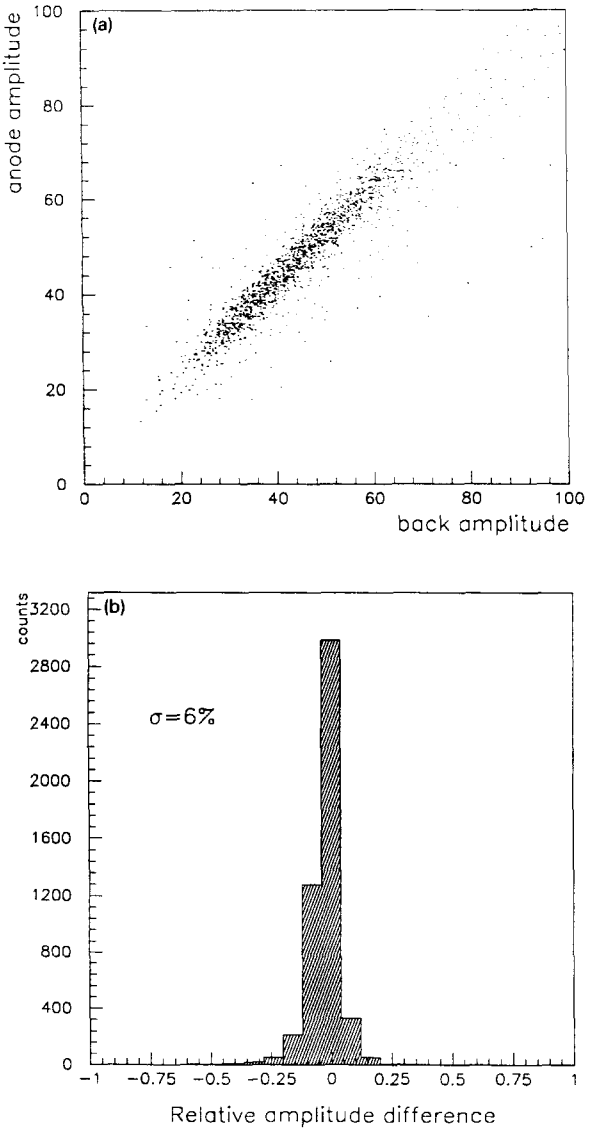

Fig. 10. (a) Scatter plot of the pulse height of the back strips vs pulse height of the anode strips. (b) Distribution of the relative differences between the pulse height on the back and on the anode strips.

4. Discussion and conclusions

The novel detector presented in this paper opens a complete set of new possibilities. One can envisage, for example, to organize the detector read-out as:

i) two high resolution projections, (X, Y) or (Z, ϕ) or small angle stereo pairs, using only one thin substrate (for example 100 μm thick);

ii) one high resolution projection (ϕ, for example) plus macroscopic pixels (> 10 mm^2) to solve ambiguities and to provide true space points;

iii) microscopic pixels (200 μm × 200 μm) plus coarse anode read-out for triggering purposes;

iv) one dimensional detector working at low voltages, i.e. in very safe conditions. In this case, the substrate could be made of low resistivity silicon, thus allowing integration of the read-out electronics on the same substrate [6].

The performances achieved with such detectors in terms of energy resolution, rate capability, X–Y reconstruction, radiation resistance, flexibility and friendliness put them in a class apart among the gas detectors.

Finally, it is important to underline that this detector could find many interesting applications also in different fields, like astrophysics, synchrotron radiation and medical imaging.

Acknowledgements

We thank G. Decarolis and C. Magazzu' of INFN-Pisa for their enthusiastic technical support.

Fig. 11. X-ray image of a tiny, swallow shaped, earring as reconstructed when the back electrode is structured in strips.

References

[1] A. Oed, Nucl. Instr. and Meth. A263 (1988) 351.
[2] F. Angelini et al., Nucl. Instr. and Meth. A283 (1989) 755.
[3] F. Angelini et al., IEEE Trans. Nucl. Sci. NS-37 (1990) 112.
[4] F. Angelini et al., CERN-PPE/91-122.
[5] F. Angelini et al., Nucl. Phys. B23A (1991) 254.
[6] F. Angelini et al., Preprint INFN PI/AE 91/19.
[7] J.A. Kadyk, Nucl. Instr. and Meth. A300 (1991) 436.
[8] H. Hartjes et al., Nucl. Instr. and Meth. A313 (1992) 377.
[9] R. Bouclier et al., CERN-PPE/91-227.
[10] T. Meyer, Proc. ECFA LHC Workshop, CERN 90-10, vol. 3 (1990) 208.